Anterior corneal profile with variable asphericity

Article *in* Applied Optics · December 2009

DOI: 10.1364/AO.48.006594 · Source: PubMed

5 authors, including:

Maria Montserrat Juarez-Aubry
Arkansas State University - Querétaro, México
6 PUBLICATIONS **42** CITATIONS

SEE PROFILE

E. Tepichin-Rodriguez
Instituto Nacional de Astrofísica, Óptica y Electrónica (INAOE)
134 PUBLICATIONS **422** CITATIONS

SEE PROFILE

Anterior corneal profile with variable asphericity

Marco A. Rosales,[1] Montserrat Juárez-Aubry,[1] Estela López-Olazagasti,[2] Jorge Ibarra,[2] and Eduardo Tepichín[2,*]

[1]Universidad de las Américas, Puebla, Ex-hacienda Santa Catarina Mártir s/n, Puebla, 72850, México

[2]Instituto Nacional de Astrofísica, Óptica y Electrónica, Luis Enrique Erro # 1, Puebla, 72840, México

*Corresponding author: tepichin@inaoep.mx

Received 24 July 2009; revised 5 November 2009; accepted 6 November 2009; posted 11 November 2009 (Doc. ID 114461); published 1 December 2009

We present a corneal profile in which the eccentricity, $e(Q = -e^2)$, has a nonlinear continuous variation from the center outwards. This nonlinear variation is intended to fit and reproduce our current experimental data in which the anterior corneal surface of the human eye exhibits different values of e at different diameters. According to our clinical data, the variation is similar to an exponential decay. We propose a linear combination of two exponential functions to describe the variation of e. We then calculate the corneal sagittal height by substituting e in the first-order aspherical surface equation to obtain the corneal profile. This corneal profile will be used as a reference to analyze the resultant profiles of the customized corneal ablation in refractive surgery.

OCIS codes: 170.4460, 170.4470, 170.4730, 330.4060, 330.5370, 330.7326.

1. Introduction

Due to the inherent complexity of the human eye, the analysis and description of its optical performance have been addressed in the literature with different approaches and simplifications, depending on the specific features to be described [1]. Within this task, several theoretical models have been proposed in which the optical surfaces of the eye are assumed to be spherical or aspherical surfaces of revolution with constant asphericity value Q [1–10]. These rotationally symmetric models also assume a constant value of the radius at the center of the cornea [11]. However, different values of Q arise within the different models [6,7]. The growing degree of complexity of the theoretical models tends to provide a more realistic description of the optical system of the eye and makes it more consistent with experimental and clinical data [10]. In addition, despite the fact that an anatomically accurate description of the human cornea needs to take into account several factors such as nonrotational–symmetric shapes, the advantages of simpler functional descriptions have been demonstrated in the literature [12–18].

On the other hand, it is well known that the corneal anterior surface makes the greatest contribution to the total refractive power of the eye [19,20]. Hence, a precise characterization of this surface is essential to the understanding of the visual performance of the eye as a physical system [21–26]. In this direction, modeling based on clinical data will improve the overall description.

As cited by Lotmar [4], R. Bonnet was able to fit experimental data into a logarithmic corneal profile. Then, by a power series approximation of the logarithmic profile, Lotmar [4] was able to compare this profile with different aspherical surfaces of different asphericity Q and constant radius at the corneal vertex. He showed that the differences between the profiles were evident below the apex of the cornea. Later on, Kiely *et al.* [20] showed that Lotmar's approximation can represent a corneal shape with constant Q and constant radius R if $Q = -0.286$. In the same paper, and as a result of clinical data [27], they obtained an average value of $Q = -0.26 \pm 0.18$ and $R = 7.72 \pm 0.27$ mm. It was also established that a value of $Q = -0.528$ is required for zero spherical aberration. But, it was recognized that this result does

0003-6935/09/356594-06$15.00/0

not take into account astigmatic corneas. Different approaches appear in the literature to address this feature [28–31]. Nevertheless, as cited by Navarro *et al.* [31], the topographies of real corneas do not match any of these ideal models. They made an interesting overview of the existing parametric models with two conic constants, Q_x and Q_y, and demonstrated that the general ellipsoid provides a better model for the normal corneas.

On the other hand, Kasprzak and Iskander [12] demonstrated that a generalized conic curve, which can be considered as the sum of two conic functions, can take into account the different values of the eccentricity in the central portion of the ophthalmic surfaces and in the periphery. However, in a recent publication Gonzalez-Méijome *et al.* [13] showed that the human cornea has different Q values for different corneal diameters. They obtained a linear variation of Q from the center towards the periphery of the normal cornea. This means that simple conic functions are not enough to describe the corneal profile.

However, according to our clinical data, the variation is similar to an exponential decay [32]. Therefore, the aim of this work is to present a corneal profile in which the eccentricity, e ($Q = -e^2$), has a nonlinear continuous variation from the center outwards. We propose a linear combination of two exponential functions to describe the variation of e. This linear combination will increase the accuracy of the reproduction of the clinical data, which cannot be achieved by a linear variation or a single exponential function. We then calculate the corneal sagittal height by substituting e in the first-order aspherical surfaces equation [33] to obtain the corneal profile. The resultant profile describes the corneal shape at different pupil diameters. This corneal profile can be used as a reference to compare the preoperated and post-operated profiles obtained with customized corneal ablation techniques [34–41].

2. Mathematical Description

A. Clinical Data

Using the refractive power and corneal analyzer Nidek ARK-10000 (Nidek Co., Ltd.), we measured the values of the eccentricity corresponding to eight distances from the optical axis—at this point we assume the anterior corneal surface to be a revolution generated surface—from a distance of 1.5 mm to 4.5 mm from the optical axis, in intervals of 0.5 mm. This procedure was applied to 71 eyes with 20/20 vision, from which we obtained some of the results illustrated in Fig. 1. The eccentricity of the rest of our sample exhibits a similar behavior. We also show in Fig. 1 two horizontal lines with the corresponding constant eccentricity value for the average normal cornea $e = 0.51$ ($Q = -0.26$), and the zero spherical aberration eccentricity value $e = 0.73$ ($Q = -0.528$). Note that regardless of the fact that in a certain interval some of the clinical data are located close to these lines, those models do not reproduce the whole set.

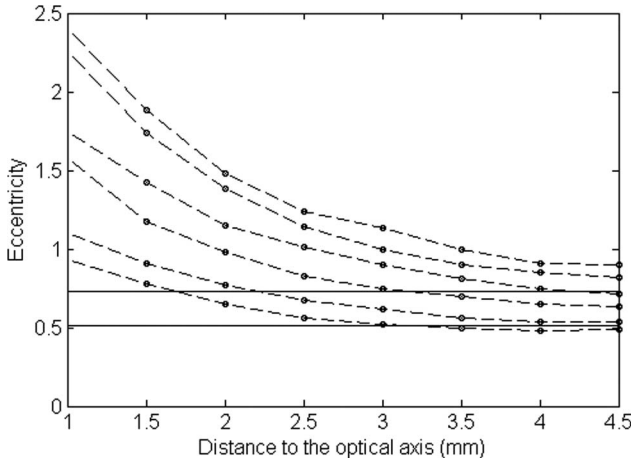

Fig. 1. Sample of our clinical data showing the variation of the eccentricity as a function of the distance to the optical axis. We also show two horizontal lines with the corresponding constant eccentricity value for the average normal cornea $e = 0.51$ ($Q = -0.26$), and the zero spherical aberration eccentricity value $e = 0.73$ ($Q = -0.528$).

As mentioned before, this means that simple conic functions are not enough to describe the corneal profile. In our case, the clinical data obtained for the eccentricity values suggest an exponential type behavior along the distance to the optical axis. However, a simple exponential function is not enough. Therefore, and as mentioned before, double-exponential decay curves are considered [32]. These linear combination increases the accuracy of the reproduction. Regarding these observations, we propose the following equation:

$$e(r) = C_1 \exp(-\lambda_1 r) + C_2 \exp(-\lambda_2 r), \qquad (1)$$

where the values of $\lambda_1, \lambda_2, C_1, C_2$, are calculated using the Nelder–Mead simplex optimization method [42] with MATLAB (MathWorks, Inc.). We first apply this two-exponential function to each one of the eye samples to see if, regardless the specific data, this function fits and reproduces each individual set. We found that despite the initial and final values of the eccentricity of each one of the individual eyes in our sample, the proposed function reproduces the experimental data within the interval with high accuracy. We initiate the fitting process with a value of λ_1, C_1 equal to 1, and λ_2, C_2 equal to 0, respectively. The criterion for terminating the optimization process is the value of the difference between two consecutive points along the radial axis, which we set to be equal to 0.001 mm. The individual values of λ_1, λ_2, C_1, and C_2 converge, up to 4 significant figures, even if we reduce the value of the criterion. The accuracy in each case was evaluated as the absolute value of the difference between the experimental value and the obtained value, which in average is less than 0.12. As an example, we show in Figs. 2(a) and 2(b) the resultant graph, together with the specific data set, for two different eyes. We display at the top of each figure the specific values of the constants in Eq. (1).

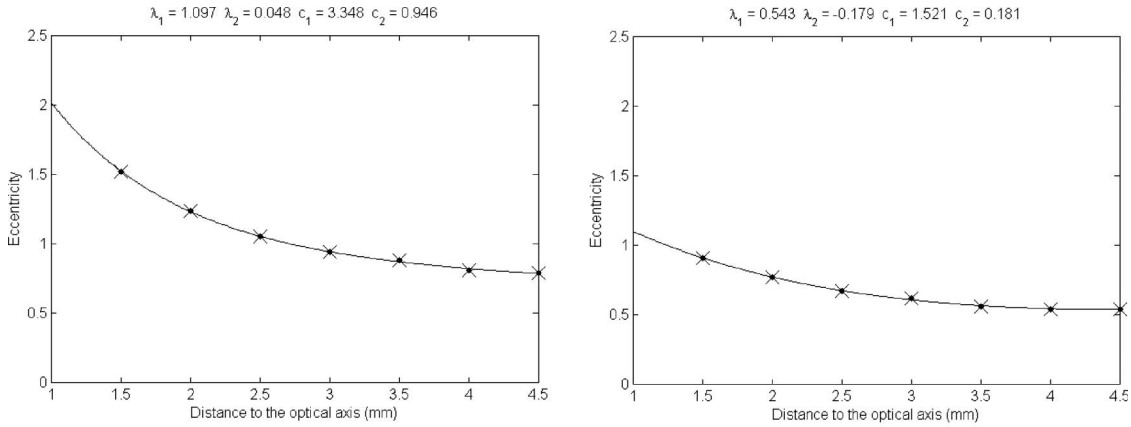

Fig. 2. (a) Data set and (b) graphical fit of two different eye samples.

In our next step, we obtained the average values of the different eccentricities for each one of the eight different distances to the optical axis to obtain the eccentricity values of the average cornea. Now, applying our proposal to the average cornea and using the same initial values for λ_1, λ_2, C_1, C_2, and the same termination criterion value as before, we obtained the graph in Fig. 3, with the following fit:

$$e(r) = 2.746\exp(-0.685r) + 0.294\exp(0.131r). \quad (2)$$

We also show in Fig. 3 the experimental average values and the corresponding standard deviation. In this case, the absolute value of the difference between the experimental data and the obtained value is less than 0.015.

We then calculate the corneal sagittal height by substituting e given in Eq. (2) into the well known first-order aspherical surfaces equation [33,43] to obtain the corneal profile.

3. Corneal Profile

In order to follow up with the mathematical evolution of the eye models in terms of Q, we start mentioning Gullstrand's model [2], in which the eye is represented by only one surface: a sector of a spherical surface, of (constant) radius R and passing through the corneal vertex. The mathematical description is based on the coordinate systems depicted in Fig. 4.

To go beyond the spherical surface, and describe the conic approximations mentioned before, we need to introduce the aspherical (nonspherical) surfaces, whose cuts containing the z axis are the conics with a nonzero, constant, eccentricity. This is expressed by introducing the asphericity or the conic coefficient $Q = -e^2$ of the surface in what is known as the first-order aspherical surfaces equation [33,43].

The general expression for such aspherical surfaces is well known [33,43]. To avoid indeterminate values of z for the different values of Q, it is usually put into the form

$$z = \frac{\frac{r^2}{R}}{1 + \sqrt{1 - (1+Q)\left(\frac{r}{R}\right)^2}}. \quad (3)$$

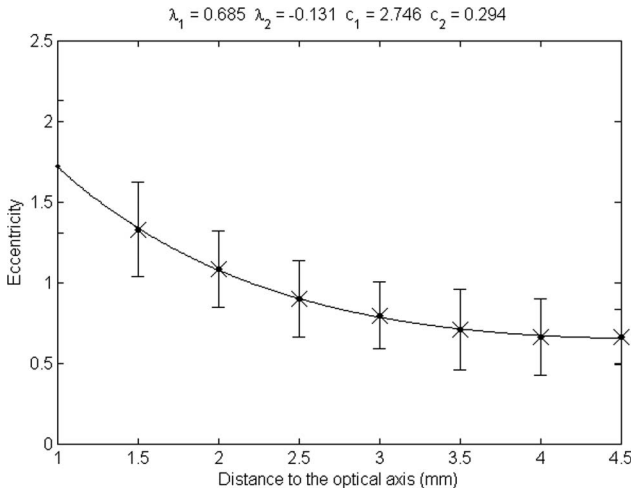

Fig. 3. Two-decay model fit for the average cornea.

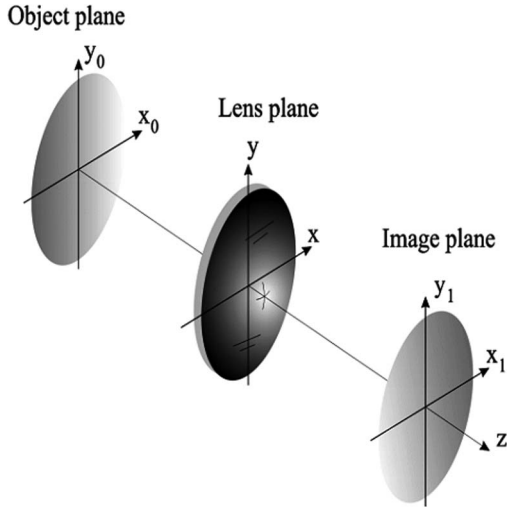

Fig. 4. Coordinate systems used for image forming systems.

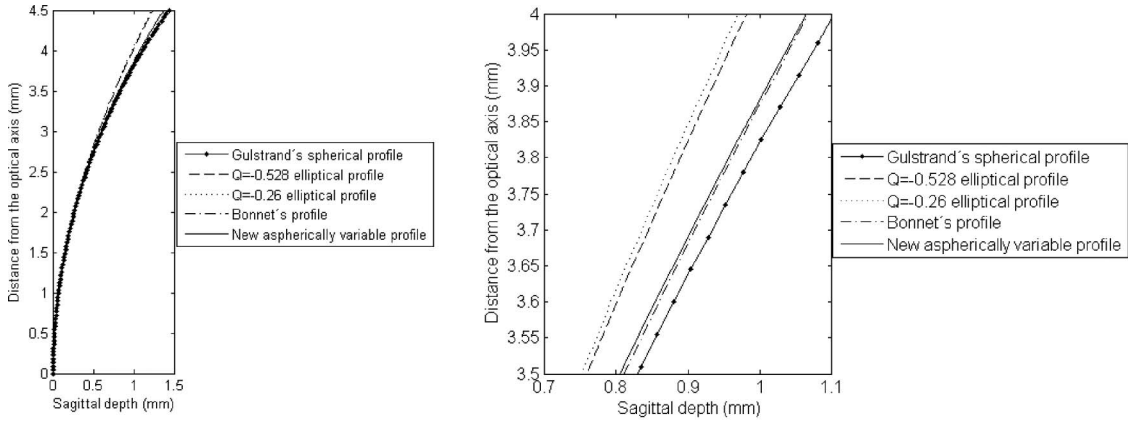

Fig. 5. (a) Comparison of the proposed aspherical profile and the conic profiles described in the text and (b) zoom in on the region where the differences between the profiles are manifest.

Now, by substituting Eq. (1) into Eq. (3) we obtain

$$z(r) = \frac{r^2}{R + (R^2 - (1 - (C_1 \exp(-\lambda_1 r) + C_2 \exp(-\lambda_2 r))r^2))^{1/2}}, \quad (4)$$

which represents the sagittal height of a generic corneal profile with variable eccentricity, i.e., asphericity. We show in Fig. 5(a) the corresponding profile of the average cornea described by the specific values given in Eq. (2). For comparison reasons, we also show Gullstrand's [2], Bonnet's [4] values and the corresponding $Q = -0.528$ and $Q = -0.26$ [20] corneal profiles mentioned before. Note that, as expected, the profiles are practically the same near the axis of the cornea, while the differences appear as we move toward the peripheral. These differences can be seen more clearly in Fig. 5(b). It is noteworthy that the proposed corneal profile is similar to Bonnet's profile; which, as mentioned before, was also obtained from clinical data.

It is straightforward to show that the differences that appear at the peripheral of the corneal models stand for the different focusing capacities of a single refractive surface formed by the rotation of these different profiles along the axis, which is in congruence with the well known fact that by modifying the corneal profile it is possible to correct refractive errors in human eyes [34–41]. Now, by rotating the proposed variable asphericity profile along the optical axis, we can obtain the 3-D profile of the corresponding anterior corneal surface. The optical axis is usually defined as the line joining the centers of curvature of the refractive surfaces, which in our case is just the anterior surface of the cornea [28]. Once we have an analytical description of the anterior corneal surface, we can move to the next step and include, for instance, the aperture stop; which is equivalent to moving from the optical axis to the visual axis. Moreover, we can include the rest of the refractive surfaces to compare the effect of letting the anterior corneal surface to vary radially. The description of the resulting corneal shape together with the corresponding focal shift will complements the typical frequency and aberration analysis of the visual performance [26,44–48].

4. Potential Applications

As mentioned before, the average corneal profile obtained with our proposal can be used as a reference to evaluate the resultant pre- and post-operated corneal profiles, as a complementary objective description to the frequency and aberration analysis of individual patients with a particular anomaly [47], as well as the individual and average performance of a set of patients with a similar defect; for instance myopic patients subjected to a pseudo-accommodative surface ablation [48]. As a first example of the potential applications, we describe the case of a 51 year old male with a pseudophakic left eye (LE), in which a miscalculated monofocal intraocular lens (IOL) was implanted 8 years earlier, who was suffering from induced hyperopia and presbyopia. Instead of trying to replace the IOL, refractive surgery with surface ablation was performed to compensate his lack of focusing. The description of the details of the applied technique is beyond the scope of this paper [34,35]. Before the surgery, the patient was asked to read targets at 6 m (far) and at 30 cm (near). With the output of these tests we obtained the information

Table 1. Pre and Post-op UCVA, BSCVA, and Manifest Refraction for Both Eyes of the Patient

LE	UCVA Far	UCVA Near	BSCVA Far	BSCVA Near
PRE	20/400	20/320	20/40 (+5.50 – 0.5 × 90)	20/40 (+2.25 ADD)
6 months	20/30	20/50	20/30 (+0.25)	20/25 (+1.00 ADD)

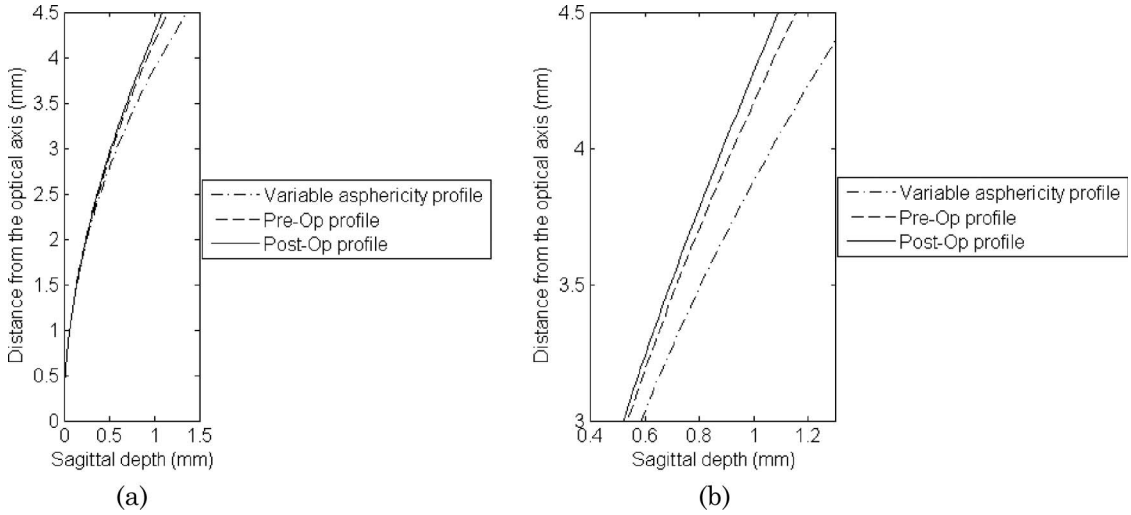

Fig. 6. (a) Pre-op and post-op corneal profiles with variable eccentricity and (b) zoom in on the region where the differences between the profiles are manifest.

of the focusing capacity of the eyes, by means of the so-called visual acuity test [35,43]. The values of the resultant uncorrected visual acuity (UCVA), the best spectacle-corrected visual acuity (BSCVA) and manifest refraction obtained for the LE are shown in the first row of Table 1. The rest of the ocular examination was unremarkable.

Typically, an UCVA of 20/20 stands for perfect vision, while 20/400 implies a legally blind person. Six months after surgery, when all the parameters seemed to stabilize, the patient showed the UCVA and BSCVA values illustrated in the second row of Table 1.

The post-op value of the UCVA implies an enhancement of the focusing capacity of the patient's LE. This enhancement can also be visualized by means of the corneal changes in the corresponding pre-op and post-op profiles. We used again the refractive power and corneal analyzer Nidek ARK-10000 mentioned above to measure the corresponding pre-op and post-op values of the eccentricity of the LE. Using Eq. (1) with the pre-op and post-op sets of eccentricity values and substituting the corresponding fit in Eq. (3), we obtained the pre-op and post-op corneal profiles shown in Fig. 6. We also show in this figure the resulting average corneal profile described by Eq. (2).

Note that, as before, the differences in the profiles are more evident at the peripheral. The difference between the post-op profile and the average corneal profile may perhaps explain the fact that the post-op visual acuity is not 20/20. The frequency and aberration analysis of this patient are beyond the scope of this paper and are left for a future paper [47].

5. Conclusions

We presented a two-exponential function suitable to describe the anterior corneal profile of the human eye with different eccentricity values at different corneal diameters. Our proposal fits and reproduces the clinical data obtained with our refractive power and corneal analyzer Nidek ARK-10000. The proposed function allowed us to obtain the average profile of a set of 71 eyes with a 20/20 visual acuity for which all the data exhibit different values of eccentricities at different corneal diameters, with an accuracy of less than 0.015. As mentioned before, the average corneal profile obtained with our proposal can be used as a reference to evaluate the resultant pre- and post-operated corneal profiles, as a complementary objective description to the frequency and aberration analysis of individual patients with a particular anomaly, as well as the individual and average performance of a set of patients with similar defects. As an example, we presented the pre-op and post-op profiles in the case of a single eye with a pseudophakic left eye, in which a miscalculated monofocal intraocular lens was implanted. The description of the resulting corneal shape together with the corresponding focal shift will complement the typical frequency and aberration analysis of the visual performance.

The authors thank Roberto Cantú, MD, and Corrección Visual con Laser for providing all the clinical data. We also thank the reviewers for useful comments that help us to improve the manuscript.

References

1. L. N. Thibos and A. Bradley, "Modeling the refractive and neuro-sensor systems of the eye," in *Visual Instrumentation: Optical Design and Engineering Principles*, P. Mouroulis, ed. (McGraw-Hill, 1999), pp. 101–159.
2. A. Gullstrand, "Apendix II," in *Handbuch der Physiologischen Optik*, Vol. 1, 3rd ed. (Voss, 1909), English translation edited by J. P. Southall (Optical Society of America, 1962), pp. 351–352.
3. Y. Le Grand, *Optique Physiologique. La Dioptrique de L'Oeil et Su Correction* (Review d'Optique, 1946).
4. W. Lotmar, "Theoretical eye model with aspherics," J. Opt. Soc. Am. **61**, 1522–1529 (1971).

5. A. C. Kooijman, "Light distribution on the retina of a wide-angle theoretical eye," J. Opt. Soc. Am. **73**, 1544–1550 (1983).
6. R. Navarro, J. Santamaría, and J. Bescós, "Accommodation-dependent model of the human eye with aspherics," J. Opt. Soc. Am. A **2**, 1273–1281 (1985).
7. H. L. Liou and N. A. Brennan, "Anatomically accurate, finite model eye for optical modeling," J. Opt. Soc. Am. A **14**, 1684–1695 (1997).
8. L. N. Thibos, M. Ye, X. Zhang, and A. Bradley, "Spherical aberration of the reduced schematic eye with elliptical refracting surface," Optom. Vis. Sci. **74**, 548–565 (1997).
9. D. A. Priest, "The development of an average, anatomically based, young adult, GRIN eye model" MSc thesis (University of Waterloo, 2004).
10. A. V. Goncharov and C. Dainty, "Wide-field schematic eye models with gradient-index lens," J. Opt. Soc. Am. A **24**, 2157–2174 (2007).
11. M. Mrochen and M. Büeler, "Asphärische Optiken: Physikalische Grundlagen," Ophthalmologe **105**, 224–233 (2008).
12. H. T. Kasprzak and D. R. Iskander, "Approximating ocular surfaces by generalised conic curves," Ophthal. Physiol. Opt. **26**, 602–609 (2006).
13. J. M. González-Méijome, C. Villa-Collar, R. Montés-Micó, and A. Gomez, "Asphericity of the human cornea with different corneal diameters," J. Cataract Refract. Surg. **33**, 465–473 (2007).
14. J. R. Jiménez, R. González Anera, and L. Jiménez del Barco, "Effects on visual function of approximations of the corneal-ablation profile during refractive surgery," Appl. Opt. **40**, 2200–2205 (2001).
15. R. G. Anera, C. Villa, J. R. Jiménez, R. Gutiérrez, and L. Jiménez del Barco, "Differences between real and predicted corneal shapes after aspherical corneal ablation," Appl. Opt. **44**, 4528–4532 (2005).
16. G. Dai, "Optical surface optimization for the correction of presbyopia," Appl. Opt. **45**, 4184–4195 (2006).
17. S. Norrby, P. Piers, C. Campbell, and M. van der Mooren, "Model eyes for evaluation of intraocular lenses," Appl. Opt. **46**, 6595–6605 (2007).
18. X. Wei and L. Thibos, "Modeling the eye's optical system by ocular wavefront tomography," Opt. Express **16**, 20490–20502 (2008).
19. Y. Le Grand and S. G. El Hague, *Physiological Optics* (Springer-Verlag, 1980).
20. P. M. Kiely, G. Smith, and L. G. Carney, "The mean shape of the human cornea," Opt. Acta **29**, 1027–1040 (1982).
21. T. O. Salmon and D. G. Horner, "Comparison of elevation, curvature, and power descriptors for corneal topographic mapping," Optom. Vis. Sci. **72**, 800–808 (1995).
22. J. Turuwhenua and J. Henderson, "A novel low-order method for recovery of the corneal shape," Optom. Vis. Sci. **81**, 863–871 (2004).
23. S. Somani, K. A. Tuan, and D. Chernyyak, "Corneal ashpericity and retinal image quality: a case study and simulations," J. Refract. Surg. **20**, S581–S585 (2004).
24. V. A. D. P. Sicam, J. Coppens, T. J. T. P. van den Berg, and R. G. L. van der Heijde, "Corneal surface reconstruction algorithm that uses Zernike polynomial representation," J. Opt. Soc. Am. A **21**, 1300–1306 (2004).
25. J. Turuwhenua, "Corneal surface reconstruction algorithm using Zernike polynomial representation: improvements," J. Opt. Soc. Am. A **24**, 1551–1561 (2007).
26. G. M. Dai, *Wavefront Optics for Vision Correction* (SPIE, 2008).
27. B. A. J. Clark, " Autocollimating photokeratoscope," J. Opt. Soc. Am. **62**, 169–176 (1972).
28. D. Atchison and G. Smith, *Optics of the Human Eye* (Butterworth-Heinemann, 2000).
29. H. Burek and W. A. Douthwaite, "Mathematical models of the general corneal surface," Ophthalmic Physiol. Opt. **13**, 68–72 (1993).
30. P. R. Preussner, J. Wahl, and C. Kramann, "Cornea model," J. Cataract Refract. Surg. **29**, 471–477 (2003).
31. R. Navarro, L. González, and J. L. Hernandez, "Optics of the average normal cornea from general and canonical representations of its surface topography," J. Opt. Soc. Am A **23**, 219–232 (2006).
32. J. Enderlein and R. Erdmann, "Fast fitting of multi-exponential decay curves," Opt. Commun. **134**, 371–378 (1997).
33. V. N. Mahajan, *Optical Imaging and Aberrations. Part 1: Ray Geometrical Optics* (SPIE, 1998), Chap. 5.
34. R. Cantú, M. A. Rosales, E. Tepichin, A. Curioca, V. Montes, and J. Bonilla, "Advanced surface ablation for presbyopia using the Nidek EC-500 Laser," J. Refract. Surg. **20**, S711–S713 (2004).
35. A. G. Bennett and R. B. Rabbetts, *Clinical Visual Optics* (Butterworths-Heinemann, 1989).
36. D. Gatinel, T. Hoang-Xuan, and D. T. Azar, "Determination of corneal asphericity after myopia surgery with the excimer laser: a mathematical model," Invest. Ophthalmol. Vis. Sci. **42**, 1736–1742 (2001).
37. D. Gatinel, J. Malet, T. Hoang-Xuan, and D. T. Azar, "Analysis of customized corneal ablations: theoretical limitations of increasing negative asphericity," Invest. Ophthalmol. Vis. Sci. **43**, 941–948 (2002).
38. J. R. Jiménez, R. G. Anera, and L. Jiménez del Barco, "Equation for corneal asphericity after corneal refractive surgery," J. Refract. Surg. **19**, 65–69 (2003).
39. D. Gatinel, J. Malet, T. Hoang-Xuan, and D. T. Azar, "Corneal asphericity change after excimer laser hyperopic surgery: theoretical effects on corneal profiles and corresponding zernike expansions," Invest. Ophthalmol. Vis. Sci. **45**, 1349–1359 (2004).
40. A. Roorda, "Human visual system—image formation," in *Encyclopedia of human imaging science and technology*, J. P. Hornack, ed. (Wiley, 2002), pp. 539–557.
41. G. M. Dai, *Wavefront Optics for Vision Correction* (SPIE, 2008).
42. E. W. Weisstein, "Nelder-Mead method in MathWorld," http://mathworld.wolfram.com/Nelder-MeadMethod.html.
43. J. Schwiegerling, *Field Guide to Visual and Ophtalmic Optics* (SPIE, 2004).
44. R. Cantú, M. A. Rosales, E. Tepichin, A. Curioca, V. Montes, and J. Bonilla, "Whole eye wavefront aberrations in Mexican male subjects," J. Refract. Surg. **20**, S685–S688 (2004).
45. E. Tepichín, R. Cantú, M. A. Rosales, S. Chavez-Cerda, D. Sánchez de la Llave, A. Curioca, V. Montes, and J. Bonilla, "PSF and MTF analysis of the visual performance in undilated Mexican normal virgin whole eyes (UCVA ≥ 20/20, 20/30 and 20/40)," Proc. SPIE **5688**, 9–18 (2005).
46. E. Tepichín-Rodriguez, R. Cantú, M. A. Rosales, D. Sánchez de la Llave, J. Ibarra-Galitzia, G. Ramírez-Zavaleta, A. Curioca, V. Montes, and J. Bonilla, "Average PSF and MTF analysis of undilated normal virgin whole eyes," Proc. SPIE **5959**, 57–64 (2005).
47. E. Tepichín, Instituto Nacional de Astrofísica, Óptica y Electrónica, Luis Enrique Erro # 1, Puebla, 72840, México, E. López-Olazagasti, M. A. Rosales, and R. Cantú are preparing a manuscript to be called "Frequency and aberration analysis of the presbyopia and residual ametropia correction after pseudophakia with monofocal IOL using a pseudo-accommodative corneal surface ablation profile."
48. A. Sinue Cruz Félix, E. López Olazagasti, M. A. Rosales, J. Ibarra, and E. Tepichín Rodríguez, "PSF and MTF comparison of two different surface ablation techniques for laser visual correction," Proc. SPIE **7443**, 7443E1 (2009).